Direct Electrical Probing of Anomalous Nernst Conductivity

Weinan Zhou[1,*], Asuka Miura[2,‡], Yuya Sakuraba[2], and Ken-ichi Uchida[2,3,†]

[1]*International Center for Young Scientists, National Institute for Materials Science, Tsukuba, 305-0047, Japan*

[2]*Research Center for Magnetic and Spintronic Materials, National Institute for Materials Science, Tsukuba, 305-0047, Japan*

[3]*Institute for Materials Research, Tohoku University, Sendai, 980-8577, Japan*

Despite the usefulness of the anomalous Nernst conductivity (α_{xy}^A) for studying electronic band structures and exploring magnetic materials with large transverse thermopower, there has not been a straightforward way to obtain α_{xy}^A in experiments. Here we propose a simple and versatile method enabling direct electrical probing of α_{xy}^A, which is realized by creating a closed circuit consisting of a target magnetic material and a nonmagnetic conductor. This method is experimentally demonstrated on a thin film of the magnetic Weyl semimetal Co_2MnGa, where the closed circuit is formed simply by our connecting both ends of the Co_2MnGa film with a Au wire. A good approximation of α_{xy}^A is obtained in a wide temperature range, validating the proposed method and showing its potential for aiding the further development of topological-materials science and transverse thermoelectrics.

I. INTRODUCTION

The anomalous Nernst conductivity, i.e., the off-diagonal component of the thermoelectric conductivity tensor (α_{xy}^A) stemming from magnetic moments, is an intrinsic material property that directly converts a longitudinal temperature gradient into a transverse electric field in a magnetic material. It has been shown that α_{xy}^A is closely linked to the Berry curvature of the electronic bands; in comparison with the anomalous Hall conductivity, which is determined by all occupied bands, α_{xy}^A can be more sensitive to the electronic band structures close to the Fermi level, rendering it a valuable tool to study the topological features of magnetic materials through transport measurements [1–18]. In addition to this rapidly increasing interest from the viewpoint of fundamental physics, α_{xy}^A is regarded as a crucial parameter to explain unconventionally large transverse thermoelectric output in some magnetic materials where the intrinsic contribution plays a dominant role. Therefore, exploring magnetic materials with large values of α_{xy}^A has become a major strategy for thermoelectric applications [19–23]. Because of the orthogonal relationship between the applied temperature gradient and the generated electric field, the transverse-thermoelectric-generation module can be a simple slab or sheet, where

no complicated three-dimensional structures are necessary, unlike conventional Seebeck-effect- (SE) based modules. Thus, transverse-thermoelectric-generation modules could potentially circumvent the problems of durability, flexibility, and cost that the SE-based modules encounter [22–26], and could be exploited for additional functionalities, such as heat-flux sensing [23,25,27,28]. Despite the significant role of α_{xy}^A in topological-materials science and transverse thermoelectrics, there has not been a straightforward way to experimentally obtain α_{xy}^A, and establishing such a method is of great importance.

The conventional experimental method for estimating α_{xy}^A consists of measurements of the anomalous Nernst effect (ANE), anomalous Hall effect (AHE), SE, and electrical resistivity of a magnetic material. The anomalous Nernst coefficient (S_{ANE}), i.e., the transverse thermopower due to the ANE, is expressed as

$$S_{ANE} = \rho_{xx}\alpha_{xy}^A - \rho_{AHE}\alpha_{xx}, \qquad (1)$$

where ρ_{xx}, ρ_{AHE}, and α_{xx} are the longitudinal resistivity, anomalous Hall resistivity, and diagonal component of the thermoelectric conductivity tensor, respectively. The first term on the right-hand side of Eq. (1) ($S_I = \rho_{xx}\alpha_{xy}^A$) is regarded as an intrinsic component of the ANE, while the second term appears as a consequence of the AHE acting on the longitudinal electric field induced by the SE, which can be rewritten as $S_{II} = -S_M \tan\theta_{AHE}$ [Fig. 1(a)], with S_M being the Seebeck coefficient of the magnetic material and $\tan\theta_{AHE} = \rho_{AHE}/\rho_{xx}$ being the anomalous Hall angle. As a result, α_{xy}^A is obtained by experimentally measuring ρ_{xx},

---

*zhou.weinan@nims.go.jp

†uchida.kenichi@nims.go.jp

‡Present address: Integrated Research for Energy and Environment Advanced Technology, Kyushu Institute of Technology, Fukuoka, 804-8550, Japan.
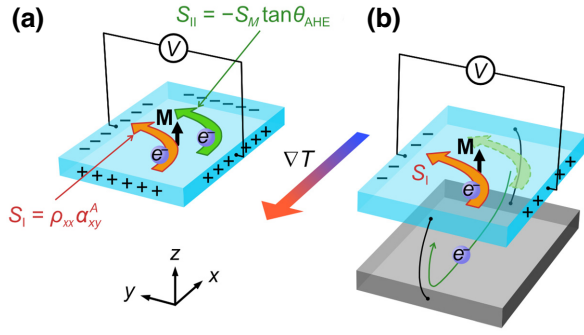
FIG. 1.   (a) The ANE in a magnetic material. The orange and green arrows represent the contribution from the S_I and S_{II} terms of S_{ANE}, while the black arrow represents the direction of magnetization (**M**). The plus and minus symbols indicate the accumulated electric charges due to the SE and the ANE. (b) The closed circuit in which a magnetic material (cyan) is electrically connected to a nonmagnetic conductor (gray) at both ends along the direction of the applied temperature gradient (∇T).

ρ_{AHE}, S_{SE}, and S_{ANE}, followed by use of Eq. (1). Many studies have used this conventional method to obtain α_{xy}^A of a variety of magnetic materials [2–5,7–19,22,23,25,28]. However, such a task could be cumbersome, and sometimes challenging to complete, since it requires various experimental techniques and measurement systems.

In this study, we propose a method to directly measure the intrinsic component of the ANE of a magnetic material and probe its α_{xy}^A with ease. This method is realized simply by creating a closed circuit consisting of the target magnetic material and a nonmagnetic conductor, and then measuring the transverse thermopower, as shown in Fig. 1(b). The formation of the closed circuit tunes the boundary conditions for electron transport, resulting in the direct emergence of α_{xy}^A reflecting the Berry curvature in the transverse thermopower. We experimentally demonstrate this method by measuring the temperature dependence of α_{xy}^A of a Co_2MnGa thin film, and compare the result with that obtained with the conventional method. The proposed method grants easy access to α_{xy}^A, and could be a useful tool in studying topological features and transverse-thermoelectric-conversion properties of magnetic materials.

II. FORMULATION

When a magnetic material is electrically connected to a nonmagnetic conductor at both ends along the direction of the applied temperature gradient (∇T), a closed circuit is formed, and its total transverse thermopower measured at the magnetic material (S_{tot}^y) is given by [29,30]

$$S_{tot}^y = S_{ANE} - \frac{\rho_{AHE}}{\rho_C/r + \rho_M}(S_C - S_M), \quad (2)$$

where ρ_C (ρ_M) and S_C (S_M) are the longitudinal resistivity and Seebeck coefficient of the nonmagnetic conductor (magnetic material), respectively. The size ratio r is determined by the geometry of the closed circuit, and in this case can be expressed as $r = (L_M/L_C) \times (A_C/A_M)$, where L_C (L_M) is the length of the nonmagnetic conductor (magnetic material) along the closed circuit [x axis in Fig. 1(b)] and A_C (A_M) is the cross-section area of the nonmagnetic conductor (magnetic material) perpendicular to the L_C (L_M) direction [y-z plane in Fig. 1(b)]. Thermoelectric materials have been connected to magnetic materials to create closed circuits so as to generate large transverse thermopower [29,31,32], which is referred to as "Seebeck-driven transverse thermoelectric generation." However, Eq. (2) is still valid when a nonmagnetic conductor with a small SE is used instead of thermoelectric materials. If we make $\rho_C/r \ll \rho_M$ through small ρ_C, large r, or both, the second term on the right-hand side of Eq. (2) is reduced to $-S_C \tan\theta_{AHE} + S_M \tan\theta_{AHE}$. Here $S_M \tan\theta_{AHE}$ cancels out the S_{II} term in S_{ANE}. If $|S_C \tan\theta_{AHE}| \ll |S_I|$, S_{tot}^y can be used to approximate S_I. In other words, the magnetic material shunted by connection to the nonmagnetic conductor leads to the disappearance of S_{II} [Fig. 1(b)]. Then α_{xy}^A can be easily obtained as

$$\alpha_{xy}^A \approx \frac{S_{tot}^y}{\rho_M}, \quad (3)$$

meaning that the simple shunting process transforms α_{xy}^A into a direct experimental observable. In comparison with the conventional method based on Eq. (1), the method proposed here reduces the number of parameters required to obtain α_{xy}^A from four to two. If ρ_M is known, a simple measurement of S_{tot}^y in the closed circuit enables the direct probing of α_{xy}^A.

III. RESULTS AND DISCUSSION

We experimentally demonstrate the proposed method using a Co_2MnGa thin film. We choose Co_2MnGa because it is a magnetic Weyl semimetal having substantial S_I and S_{II} terms contributing to its large S_{ANE} [7,11,14,15]. The 26-nm-thick Co_2MnGa thin film is epitaxially deposited on a single-crystal MgO(100) substrate at room temperature by magnetron sputtering, followed by postannealing at $500\,°C$. After the sample is cooled to room temperature, a 2-nm-thick Al capping layer is deposited to prevent oxidization. To study the structure of the Co_2MnGa thin film, we measure its X-ray-diffraction (XRD) patterns with Cu $K\alpha$ radiation, which indicates an epitaxial growth of Co_2MnGa (see Supplemental Material [33] for XRD patterns of the thin film). From these results, we obtain the integrated-intensity ratio between the 111 and 444 peaks ($I_{111}^{exp}/I_{444}^{exp}$) and between the 002 and 004 peaks ($I_{002}^{exp}/I_{004}^{exp}$). These values are compared with the

simulated integrated-intensity ratio ($I_{111}^{sim}/I_{444}^{sim}$ and $I_{002}^{sim}/I_{004}^{sim}$) for a perfectly $L2_1$-ordered structure. The details of the simulation are described in Ref. [15]. The degree of $L2_1$ order ($\sqrt{(I_{111}^{exp}/I_{444}^{exp})/(I_{111}^{sim}/I_{444}^{sim})}$) is estimated to be 0.70 for the Co$_2$MnGa thin film, while its degree of B2 order ($\sqrt{(I_{002}^{exp}/I_{004}^{exp})/(I_{002}^{sim}/I_{004}^{sim})}$) is estimated to be 0.74. The composition of Co$_2$MnGa is determined to be Co$_{45.7}$Mn$_{25.4}$Ga$_{28.9}$ by X-ray-fluorescence spectroscopy. We then pattern the Co$_2$MnGa film into a 2-mm-wide and 8-mm-long Hall-bar structure using photolithography and Ar-ion milling, followed by the formation of Ta(2 nm)/Au(50 nm) electrodes and on-chip thermometers through a lift-off process. The on-chip thermometers are placed at the positions corresponding to the electrodes of the Hall bar along the x axis, as shown in Fig. 2(a).

To create the closed circuit, we simply connect both ends of the Co$_2$MnGa film along the x axis with a 30-μm-diameter Au bonding wire. Here Co$_2$MnGa is the magnetic material under study, while the Au wire serves as the nonmagnetic conductor. Besides the convenience of using the Au wire, its small ρ_C (2.3 μΩ cm at room temperature) and small S_C (between 0.7 and 2.0 μV K^{-1} for the temperature range measured in this study [35]) make it a good nonmagnetic conductor for the proposed method. To measure the transverse thermopower, we set the sample on a homemade holder having a structure similar to the one used in the work reported in Ref. [36], which can generate a temperature gradient (∇T) along the x axis in the sample. During the measurement, the holder is placed in a Physical Property Measurement System (PPMS), which is used to control the temperature (T) and magnetic field (H) (see the Appendix for details of the thermoelectric measurement setup). ρ_M and ρ_{AHE} of Co$_2$MnGa as a function of T are also obtained by our measuring the reference sample, where the Au wire connecting both ends of the Co$_2$MnGa film is removed.

Figures 2(b) and 2(c) show the magnetic field dependence of the transverse electric field (E^y) divided by ∇T for the closed-circuit and reference samples, respectively, measured with the temperature of the PPMS set at 300 K. The observed signal of the reference sample shows the H-odd dependence and saturation at $|\mu_0 H| \sim 1$ T, which is attributed to the ANE of Co$_2$MnGa in the open-circuit condition. By contrast, the signal of the closed-circuit sample is smaller than that of the reference sample, although the shapes are similar to each other. The curve in Fig. 2(b) also saturates at $|\mu_0 H| \sim 1$ T along the z axis, suggesting the transverse thermopower of the closed-circuit sample is determined by the magnetization (**M**) of Co$_2$MnGa as well. Figure 2(d) shows the magnetic field dependence of ρ_{yx} of Co$_2$MnGa measured at 300 K, where the signal is mostly due to the AHE. The S_{tot}^y, S_{ANE}, and ρ_{AHE} values are evaluated by our extrapolating the curves in Figs. 2(b)–2(d)
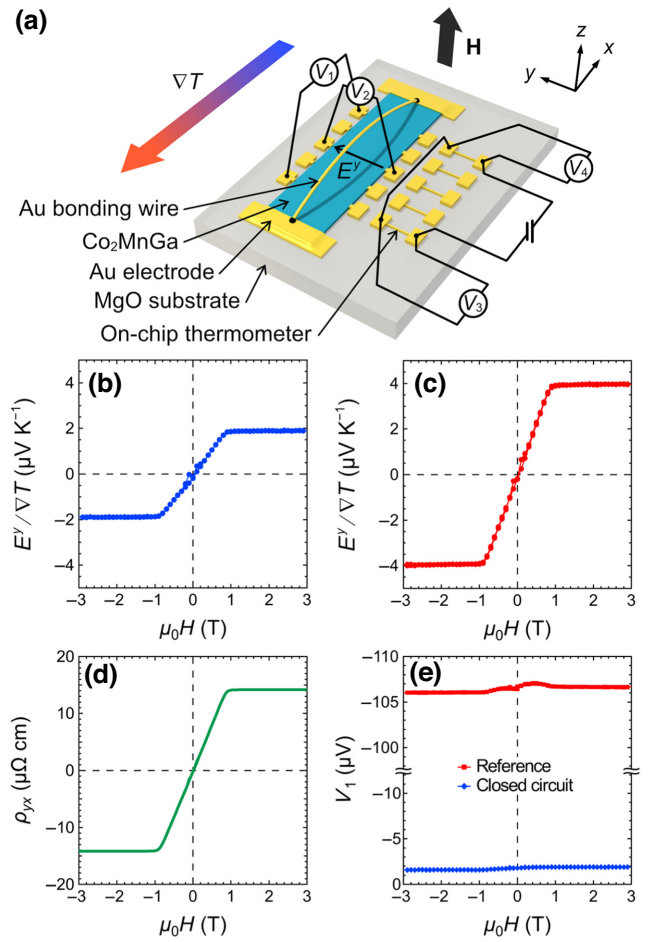

FIG. 2. (a) The sample structure and measurement setup for the experimental demonstration of the proposed method to directly probe α_{xy}^A. V_1, V_2, V_3, and V_4 represent four nano-voltmeters measuring the longitudinal thermoelectric signal, transverse thermoelectric signal, and resistance of two on-chip thermometers, respectively. (b),(c) Magnetic field (H) dependence of the transverse electric field (E^y) divided by ∇T for the closed-circuit sample (b) and the reference sample (c), measured with the temperature of the PPMS set at 300 K. (d) Magnetic field dependence of the transverse resistivity (ρ_{yx}) of the reference sample at 300 K, showing the AHE of Co$_2$MnGa. (e) Magnetic field dependence of the voltage from V_1 of the closed-circuit (blue diamonds) and reference (red squares) samples, measured during the acquisition of the results in (b),(c), respectively. The magneto-Seebeck effect [34] in Co$_2$MnGa is found to be negligibly small.

at high magnetic field after the saturation of magnetization down to zero magnetic field. Figure 2(e) shows the longitudinal thermopower from V_1 measured at the same time when the results in Figs. 2(b) and 2(c) are obtained. In the case of the reference sample, this voltage is due to the SE of the Co$_2$MnGa-Au thermocouple (note that similar Au bonding wires are used to connect the electrodes of

the sample to the homemade holder), and S_M can be calculated by dividing the voltage at zero magnetic field by the corresponding temperature difference and then adding S_C of Au. On the other hand, the magnitude of the longitudinal thermopower of the closed-circuit sample is dramatically reduced, indicating that the SE of Co_2MnGa is indeed shunted by the connection to the Au wire at both ends. The results measured with the temperature of the PPMS set at different values are given in Supplemental Material [33].

By applying Eq. (3) to the experimental results for the closed-circuit sample, we are able to probe α_{xy}^A of Co_2MnGa with ease. The values obtained with the proposed method and the conventional method are compared in Fig. 3, where the data points are plotted at T obtained during the measurement of the transverse thermopower. The corresponding ρ_M and ρ_{AHE} of Co_2MnGa at T are calculated with use of data points just above and below T with the assumption of a linear change with temperature. Figure 4 summarizes the temperature dependence of various parameters of Co_2MnGa obtained by our measuring the reference sample. These results are necessary to obtain α_{xy}^A by the conventional method. As one can see in Fig. 3(a), S_{tot}^y approximates S_I nicely and shows the same temperature dependence, with the values being slightly smaller than S_I. The same can be said for the comparison between α_{xy}^A and S_{tot}^y/ρ_M. A logarithmic temperature dependence of α_{xy}^A/T has been considered strong evidence for the Weyl magnet Co_2MnGa [7], which can be clearly seen in the inset in Fig. 3(b) for both α_{xy}^A/T and $S_{tot}^y/\rho_M T$ in the same temperature range above approximately 150 K. The comparisons thus demonstrate the usefulness of the proposed method in a wide temperature range.

To understand the small difference in results between the two methods and gain insight into the conditions to have a good approximation with use of the proposed method, we focus on the transverse thermopower and calculate $S_{tot}^y - S_I$ in the parameter space of the size ratio r and $\tan\theta_{AHE}$, as shown in Fig. 5(a), where we use the measured parameters of Co_2MnGa and S_C of Au at $T = 305$ K for the calculation, except ρ_{AHE} (consequently $\tan\theta_{AHE}$), which is a varying parameter. Thus, $S_{tot}^y - S_I$ is equivalent to $(-S_M \tan\theta_{AHE}) - \frac{\rho_{AHE}}{\rho_C/r + \rho_M}(S_C - S_M)$ based on Eqs. (1) and (2). The white area in Fig. 5(a) represents $S_{tot}^y - S_I = 0$, while the red (blue) area represents S_{tot}^y being larger (smaller) than S_I. The dashed black line indicates $\tan\theta_{AHE}$ of Co_2MnGa measured in the experiment, with the curve displayed in Fig. 5(b). $S_{tot}^y - S_I$ from the experimental results at $T = 305$ K is shown as a blue data point in Fig. 5(b), where good agreement between experiment and calculation can be seen. When r is small, S_{tot}^y approaches S_{ANE}, and $S_{tot}^y - S_I$ approaches S_{II} (note that S_{II} increases as $\tan\theta_{AHE}$ is artificially increased). As r increases to more than 1 in Fig. 5(a), $S_{tot}^y - S_I$ decreases

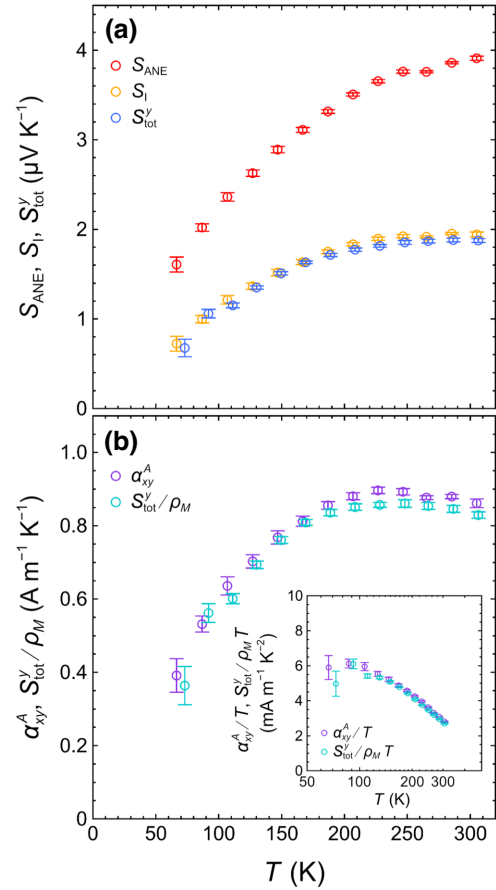FIG. 3. (a) S_{ANE} and S_I of the reference sample in comparison with S_{tot}^y of the closed-circuit sample as a function of T. (b) α_{xy}^A obtained with the conventional method and S_{tot}^y/ρ_M, which approximately corresponds to α_{xy}^A through Eq. (3). The inset in (b) shows α_{xy}^A/T and $S_{tot}^y/\rho_M T$ as a function of logarithmic T.

and converges to $-S_C \tan\theta_{AHE}$. For most magnetic materials having $\tan\theta_{AHE} < 0.1$ [37], the value of this difference would be on the scale of -0.1 μV K^{-1}. If the measured S_{tot}^y is much larger than this value, such as in Co_2MnGa, the proposed method can realize a good approximation of α_{xy}^A. If S_{tot}^y is close to this value, the proposed method is not able to properly evaluate α_{xy}^A, but it can still serve as an indication of small S_I and α_{xy}^A. Meanwhile, if the target material has an exceptionally large $\tan\theta_{AHE}$, the difference would increase proportionally, although this difference can be further reduced by use of a nonmagnetic conductor with smaller S_C. In contrast, the change of $S_{tot}^y - S_I$ along the horizontal axis in Fig. 5(a) is much-more prominent, suggesting that a proper r is important for the proposed method. Here $r > 1$ would be sufficient for $S_{tot}^y - S_I$ to reach $-S_C \tan\theta_{AHE}$, which corresponds to $(\rho_C/r)/\rho_M < 1/100$.

As shown above, the proposed method can be easily implemented in the experiment to directly access S_I of a
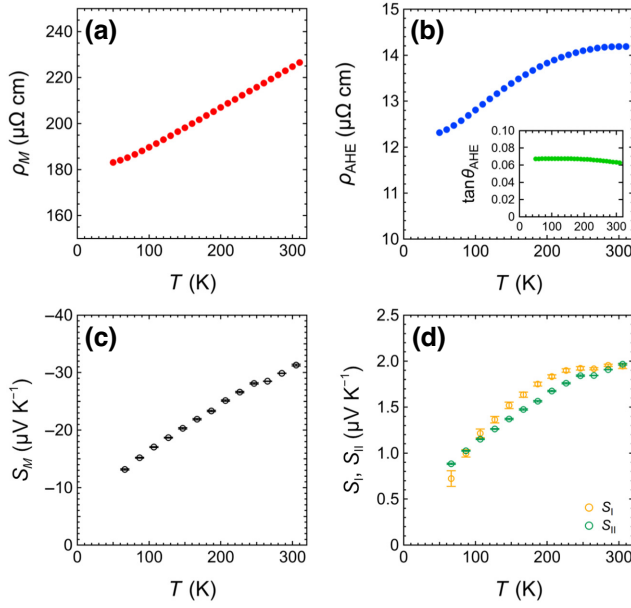
FIG. 4. (a) ρ_M, (b) ρ_{AHE}, and (c) S_M of the Co$_2$MnGa thin film as a function of T obtained by our measuring the reference sample. The inset in (b) shows $\tan\theta_{AHE}$ as a function of T. (d) The S_I and S_{II} terms of the Co$_2$MnGa thin film as a function of T calculated by the conventional method.

FIG. 5. (a) Calculated $S^y_{tot} - S_I$ in the parameter space of the size ratio r and $\tan\theta_{AHE}$, with other parameters obtained in the experiment at $T = 305$ K. Dark red means that $S^y_{tot} - S_I >$ $2\ \mu$V K^{-1}. (b) $S^y_{tot} - S_I$ as a function of r with use of $\tan\theta_{AHE}$ of Co$_2$MnGa measured in the experiment, which corresponds to the dashed black line in (a). The blue data point represents $S^y_{tot} - S_I$ from the experimental results.

magnetic material through the measurement of S^y_{tot} and to probe its α^A_{xy} with knowledge of only ρ_M, in contrast to four different parameters required by the conventional method. This could reduce the number of measurements and ease the requirement on the experimental setup although the process of measuring S^y_{tot} (applying a temperature gradient to the sample and varying H) is the same as that of measuring S_{ANE}. The accurate evaluation of S_M is often difficult due to parasitic thermoelectric signals from electrical wires connected to the sample, and S_M no longer being necessary in the proposed method could be especially beneficial to probe α^A_{xy}. Fewer parameters would mean fewer errors propagating to α^A_{xy}, which could increase the reproductivity and reliability of the results. These advantages of the proposed method are especially beneficial for high-throughput materials research to determine if a candidate material has large α^A_{xy}. In addition, use of the first-principles calculations to obtain the Berry curvature and derive α^A_{xy} has been popularized in recent years and plays an important role in exploiting and predicting materials with valuable properties. The proposed method could make α^A_{xy} a direct observable in the experiment, thereby enabling fast and straightforward comparison with the theory and promoting further understanding of the matter. It is worth mentioning that although the experimental demonstration is done on a magnetic thin film, the proposed method should also be applicable to study bulk materials, as long as the required condition of $\rho_C/r \ll \rho_M$ is met.
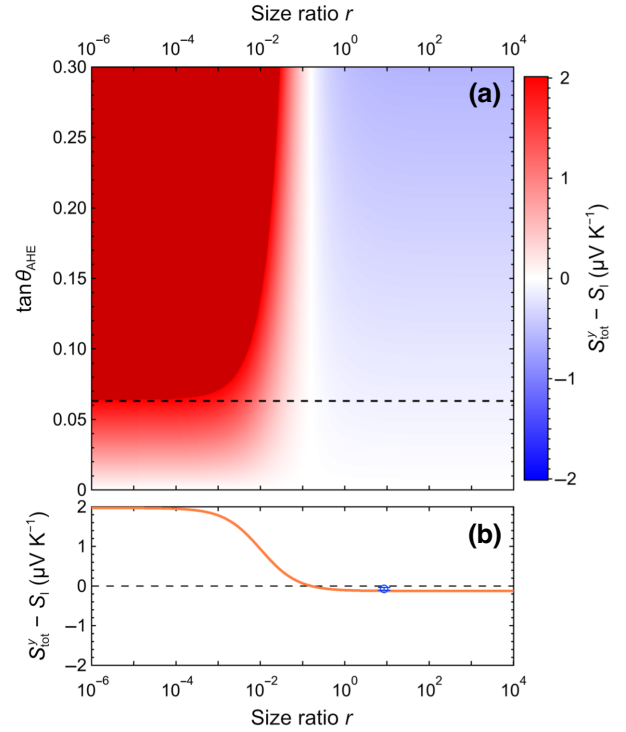
IV. CONCLUSION

We propose a method to directly probe α^A_{xy} of a magnetic material that is realized simply by connecting both ends of the magnetic material along the direction of the temperature gradient with a nonmagnetic conductor to create a closed circuit. S^y_{tot} of the closed circuit approximates the S_I term of the magnetic material, and α^A_{xy} can be easily obtained from S^y_{tot} and ρ_M, in contrast to four different parameters being required in the conventional method. The proposed method is experimentally demonstrated to probe the temperature dependence of α^A_{xy} of a Co$_2$MnGa thin film. The closed circuit is easily realized with use of a Au wire, and a good approximation is obtained for both S_I and α^A_{xy} in the entire temperature range between 70 and 305 K, validating this method. Proper conditions to achieve a good approximation are also discussed, providing guides for the use of the proposed method. As the use of α^A_{xy} is growing in popularity, our finding could become a powerful tool propelling studies of topological-materials science and application of transverse thermoelectric phenomena.

APPENDIX: THERMOELECTRIC MEASUREMENT SETUP

For the thermoelectric measurements, we use a homemade holder, which is built upon a commercially available multifunction probe and an empty sample puck. One side of the sample is thermally connected to a Cu block and then to the puck, which serves as a heat sink; the other side is thermally connected to a heater through another Cu block, while being insulated from the puck by a Bakelite plate. This structure to generate a temperature gradient (∇T) in a thin-film sample is similar to the one used in the work reported in Ref. [36] (see Supplemental Material [33] for a photograph of the thermoelectric measurement setup). To measure the electrical signals from the sample, the same Au bonding wires are used to connect the electrodes on the samples to the electrodes on the holder. These electrical connections then go to the other end of the multifunction probe through Cu wires, and eventually out of the probe and into a connection box to meet with the cables from external electronics. The electrodes on the holder are thermally anchored to the heat sink. During thermoelectric measurements, the homemade holder is placed in a PPMS (VersaLab made by Quantum Design). The heater is electrically connected to the pins at the bottom of the PPMS. These connections then go through the cables inside the PPMS and eventually feed to an external source meter (Keithley 2401 SourceMeter). Another source meter of the same type is used to apply 100 μA to the on-chip thermometers. Together with two nanovoltmeters [V_3 and V_4 in Fig. 2(a); Keithley 2182A nanovoltmeter], we are able to accurately measure the resistance of on-chip thermometers by the four-terminal method. Meanwhile, two nanovoltmeters of the same type [V_1 and V_2 in Fig. 2(a)] are used to measure the longitudinal and transverse thermoelectric signals from the sample. All the external electronics are controlled by a personal computer through general-purpose-interface-bus cables, while this personal computer also communicates with a personal computer that controls the temperature (T) and magnetic field (H) of the PPMS. Before generation of the temperature gradient in the sample, the on-chip thermometers are calibrated by our measuring their resistance as a function of temperature

under zero magnetic field. Then we set the temperature of the PPMS to a certain value, generate a temperature gradient in the sample, and sweep the magnetic field along the z axis while monitoring the longitudinal and transverse thermoelectric signals from the closed circuit with two nanovoltmeters: V_1 and V_2, respectively. The resistance of the on-chip thermometers is also measured and subsequently converted to temperature; the difference is divided by the distance between the two thermometers (4 mm) to work out the value of ∇T, while the average is used as the temperature for the obtained S_{tot}^{y}. The temperature of the PPMS is varied between 60 and 300 K with a 20-K interval. The same measuring process is conducted on the reference sample, where the Au wire connecting both ends of the Co_2MnGa film is removed; this is the conventional ANE measurement.

---

[1] D. Xiao, Y. Yao, Z. Fang, and Q. Niu, Berry-Phase Effect in Anomalous Thermoelectric Transport, Phys. Rev. Lett. **97**, 026603 (2006).

[2] T. Miyasato, N. Abe, T. Fujii, A. Asamitsu, S. Onoda, Y. Onose, N. Nagaosa, and Y. Tokura, Crossover Behavior of the Anomalous Hall Effect and Anomalous Nernst Effect in Itinerant Ferromagnets, Phys. Rev. Lett. **99**, 086602 (2007).

[3] Y. Pu, D. Chiba, F. Matsukura, H. Ohno, and J. Shi, Mott Relation for Anomalous Hall and Nernst Effects in $Ga_{1-x}Mn_xAs$ Ferromagnetic Semiconductors, Phys. Rev. Lett. **101**, 117208 (2008).

[4] X. Li, L. Xu, L. Ding, J. Wang, M. Shen, X. Lu, Z. Zhu, and K. Behnia, Anomalous Nernst and Righi-Leduc Effects in Mn_3Sn: Berry Curvature and Entropy Flow, Phys. Rev. Lett. **119**, 056601 (2017).

[5] M. Ikhlas, T. Tomita, T. Koretsune, M.-T. Suzuki, D. Nishio-Hamane, R. Arita, Y. Otani, and S. Nakatsuji, Large anomalous Nernst effect at room temperature in a chiral antiferromagnet, Nat. Phys. **13**, 1085 (2017).

[6] J. Noky, J. Gooth, C. Felser, and Y. Sun, Characterization of topological band structures away from the Fermi level by the anomalous Nernst effect, Phys. Rev. B **98**, 241106(R) (2018).

[7] A. Sakai, Y. P. Mizuta, A. A. Nugroho, R. Sihombing, T. Koretsune, M.-T. Suzuki, N. Takemori, R. Ishii, D. Nishio-Hamane, R. Arita, P. Goswami, and S. Nakatsuji, Giant anomalous Nernst effect and quantum-critical scaling in a ferromagnetic semimetal, Nat. Phys. **14**, 1119 (2018).

[8] S. N. Guin, P. Vir, Y. Zhang, N. Kumar, S. J. Watzman, C. Fu, E. Liu, K. Manna, W. Schnelle, J. Gooth, C. Shekhar, Y. Sun, and C. Felser, Zero-field Nernst effect in a ferromagnetic kagome-lattice Weyl-semimetal $Co_3Sn_2S_2$, Adv. Mater. **31**, 1806622 (2019).

[9] L. Ding, J. Koo, L. Xu, X. Li, X. Lu, L. Zhao, Q. Wang, Q. Yin, H. Lei, B. Yan, Z. Zhu, and K. Behnia, Intrinsic Anomalous Nernst Effect Amplified by Disorder in a Half-Metallic Semimetal, Phys. Rev. X **9**, 041061 (2019).

[10] C. Wuttke, F. Caglieris, S. Sykora, F. Scaravaggi, A. U. B. Wolter, K. Manna, V. Süss, C. Shekhar, C. Felser, B.

Büchner, and C. Hess, Berry curvature unravelled by the anomalous Nernst effect in Mn_3Ge, Phys. Rev. B **100,** 085111 (2019).

[11] S. N. Guin, K. Manna, J. Noky, S. J. Watzman, C. Fu, N. Kumar, W. Schnelle, C. Shekhar, Y. Sun, J. Gooth, and C. Felser, Anomalous Nernst effect beyond the magnetization scaling relation in the ferromagnetic Heusler compound Co_2MnGa, NPG Asia Mater. **11,** 16 (2019).

[12] H. Yang, W. You, J. Wang, J. Huang, C. Xi, X. Xu, C. Cao, M. Tian, Z.-A. Xu, J. Dai, and Y. Li, Giant anomalous Nernst effect in the magnetic Weyl semimetal $Co_3Sn_2S_2$, Phys. Rev. Mater. **4,** 024202 (2020).

[13] Y. Sakuraba, K. Hyodo, A. Sakuma, and S. Mitani, Giant anomalous Nernst effect in the $Co_2MnAl_{1-x}Si_x$ Heusler alloy induced by Fermi level tuning and atomic ordering, Phys. Rev. B **101,** 134407 (2020).

[14] L. Xu, X. Li, L. Ding, T. Chen, A. Sakai, B. Fauqué, S. Nakatsuji, Z. Zhu, and K. Behnia, Anomalous transverse response of Co_2MnGa and universality of the room-temperature $\alpha_{ij}^A/\sigma_{ij}^A$ ratio across topological magnets, Phys. Rev. B **101,** 180404(R) (2020).

[15] K. Sumida, Y. Sakuraba, K. Masuda, T. Kono, M. Kakoki, K. Goto, W. Zhou, K. Miyamoto, Y. Miura, T. Okuda, and A. Kimura, Spin-polarized Weyl cones and giant anomalous Nernst effect in ferromagnetic Heusler films, Commun. Mater. **1,** 89 (2020).

[16] T. Asaba, V. Ivanov, S. M. Thomas, S. Y. Savrasov, J. D. Thompson, E. D. Bauer, and F. Ronning, Colossal anomalous Nernst effect in a correlated noncentrosymmetric kagome ferromagnet, Sci. Adv. **7,** eabf1467 (2021).

[17] Y. Pan, C. Le, B. He, S. J. Watzman, M. Yao, J. Gooth, J. P. Heremans, Y. Sun, and C. Felser, Giant anomalous Nernst signal in the antiferromagnet $YbMnBi_2$, Nat. Mater. **21,** 203 (2022).

[18] H. Zhang, J. Koo, C. Xu, M. Sretenovic, B. Yan, and X. Ke, Exchange-biased topological transverse thermoelectric effects in a kagome ferrimagnet, Nat. Commun. **13,** 1091 (2022).

[19] H. Nakayama, K. Masuda, J. Wang, A. Miura, K. Uchida, M. Murata, and Y. Sakuraba, Mechanism of strong enhancement of anomalous Nernst effect in Fe by Ga substitution, Phys. Rev. Mater. **3,** 114412 (2019).

[20] A. Miura, H. Sepehri-Amin, K. Masuda, H. Tsuchiura, Y. Miura, R. Iguchi, Y. Sakuraba, J. Shiomi, K. Hono, and K. Uchida, Observation of anomalous Ettingshausen effect and large transverse thermoelectric conductivity in permanent magnets, Appl. Phys. Lett. **115,** 222403 (2019).

[21] J. Noky, Y. Zhang, J. Gooth, C. Felser, and Y. Sun, Giant anomalous Hall and Nernst effect in magnetic cubic Heusler compounds, npj Comput. Mater. **6,** 77 (2020).

[22] A. Sakai, S. Minami, T. Koretsune, T. Chen, T. Higo, Y. Wang, T. Nomoto, M. Hirayama, S. Miwa, D. Nishio-Hamane, F. Ishii, R. Arita, and S. Nakatsuji, Iron-based binary ferromagnets for transverse thermoelectric conversion, Nature **581,** 53 (2020).

[23] K. Uchida, W. Zhou, and Y. Sakuraba, Transverse thermoelectric generation using magnetic materials, Appl. Phys. Lett. **118,** 140504 (2021).

[24] Y. Sakuraba, K. Hasegawa, M. Mizuguchi, T. Kubota, S. Mizukami, T. Miyazaki, and K. Takanashi, Anomalous Nernst effect in $L1_0$-FePt/MnGa thermopiles for new thermoelectric applications, Appl. Phys. Express **6,** 033003 (2013).

[25] W. Zhou and Y. Sakuraba, Heat flux sensing by anomalous Nernst effect in Fe–Al thin films on a flexible substrate, Appl. Phys. Express **13,** 043001 (2020).

[26] K. Uchida and J. P. Heremans, Thermoelectrics: From longitudinal to transverse, Joule **6,** 2240 (2022).

[27] T. Higo, Y. Li, K. Kondou, D. Qu, M. Ikhlas, R. Uesugi, D. Nishio-Hamane, C. L. Chien, Y. Otani, and S. Nakatsuji, Omnidirectional control of large electrical output in a topological antiferromagnet, Adv. Funct. Mater. **31,** 2008971 (2021).

[28] R. Modak, Y. Sakuraba, T. Hirai, T. Yagi, H. Sepehri-Amin, W. Zhou, H. Masuda, T. Seki, K. Takanashi, T. Ohkubo, and K. Uchida, Sm-Co-based amorphous alloy films for zero-field operation of transverse thermoelectric generation, Sci. Technol. Adv. Mater. **23,** 767 (2022).

[29] W. Zhou, K. Yamamoto, A. Miura, R. Iguchi, Y. Miura, K. Uchida, and Y. Sakuraba, Seebeck-driven transverse thermoelectric generation, Nat. Mater. **20,** 463 (2021).

[30] K. Yamamoto, R. Iguchi, A. Miura, W. Zhou, Y. Sakuraba, Y. Miura, and K. Uchida, Phenomenological analysis of transverse thermoelectric generation and cooling performance in magnetic/thermoelectric hybrid systems, J. Appl. Phys. **129,** 223908 (2021).

[31] W. Zhou, T. Hirai, K. Uchida, and Y. Sakuraba, Seebeck-driven transverse thermoelectric generation in on-chip devices, J. Phys. D: Appl. Phys. **55,** 335002 (2022).

[32] W. Zhou, A. Miura, T. Hirai, Y. Sakuraba, and K. Uchida, Seebeck-driven transverse thermoelectric generation in magnetic hybrid bulk materials, Appl. Phys. Lett. **122,** 062402 (2023).

[33] See Supplemental Material http://link.aps.org/supplemental/10.1103/PhysRevApplied.19.064079 for X-ray-diffraction patterns of the thin film, a photograph of the thermoelectric measurement setup, and additional transport-measurement results.

[34] K. Uchida, Transport phenomena in spin caloritronics, Proc. Jpn. Acad. Ser. B **97,** 69 (2021).

[35] I. S. Grigoriev and E. Z. Meilikhov, *Handbook of Physical Quantities* (CRC, Boca Raton, 1997).

[36] J. Wang, Y.-C. Lau, W. Zhou, T. Seki, Y. Sakuraba, T. Kubota, K. Ito, and K. Takanashi, Strain-induced large anomalous Nernst effect in polycrystalline Co_2MnGa/AlN multilayers, Adv. Electron. Mater. **8,** 2101380 (2022).

[37] J. Karel, D. S. Bouma, C. Fuchs, S. Bennett, P. Corbae, S. B. Song, B. H. Zhang, R. Q. Wu, and F. Hellman, Unexpected dependence of the anomalous Hall angle on the Hall conductivity in amorphous transition metal thin films, Phys. Rev. Mater. **4,** 114405 (2020).